Journal of Electroceramics, 13, 653–661, 2004

Cathodic Polarization Study on Doped Lanthanum Gallate Electrolyte Using Impedance Spectroscopy

WENQUAN GONG, SRIKANTH GOPALAN & UDAY B. PAL

Department of Manufacturing Engineering, Boston University, 15 St. Mary's Street, Boston, Massachusetts 02215, USA

Submitted July 2, 2003; Revised February 27, 2004; Accepted March 3, 2004

Abstract. The perovskite electrolyte $La_{1-x}Sr_xGa_{1-y}Mg_yO_3$ (LSGM) has received a lot of interest in recent years after it was first reported to have significantly higher oxygen-ion conductivity than conventional YSZ. A very large fraction of the total polarization losses in SOFC is known to occur at the electrode-electrolyte interfaces manifesting itself as the kinetic barrier to charge-transfer reactions. AC complex impedance spectroscopy studies were conducted on symmetrical cells of the type [air, electrode/LSGM electrolyte/electrode, air] to measure the charge-transfer polarization at the cathode-electrolyte interfaces. The electrode materials were slurry-coated on both sides of the LSGM electrolyte support. The cathode materials investigated in this study include $La_{1-x}Sr_xMnO_3$(LSM), LSCF ($La_{1-x}Sr_xCo_yFe_{1-y}O_3$) and a two-phase particulate composite consisting of LSM +doped-lanthanum gallate (LSGM). Symmetrical cell studies were also performed on SOFC anode materials. The principal anode material investigated in this study is a porous composite of Ni-gadolinium doped ceria (GDC). It is well known that Ni reacts with the state-of-the-art LSGM anode material. Thus our approach is to use a barrier layer of GDC between the Ni-GDC anode and the LSGM electrolyte. This paper will focus on the influence of microstructure, electrode composition, electrode thickness, interfacial compatibility and electrode processing conditions on cathode and anode polarization.

Keywords: solid oxide fuel cell, cathode, anode, polarization, lanthanum gallate, perovskite, electrolyte

Introduction

Solid oxide fuel cells (SOFCs) offer the possibility of very high efficiency power generation. They are noiseless, emit far lower quantities of greenhouse gases such as CO_2 compared to conventional power generation systems, have virtually zero NO_x and SO_x emissions. Despite their many advantages, SOFC power systems are not yet cost-effective to merit large-scale deployment in the power generation industry. Of the approaches currently being investigated to decrease the cost of SOFCs, improving power density while decreasing operating temperature is perhaps the most promising option. Improvements in power density will result in decreased system size, which in turn will have the effect of decreasing the size of the balance of plant (BOP). Decreasing operating temperature will lead to the deployment of cheaper manifolding and interconnection materials. However, decreasing operating temperature has the effect of increasing all types of polarization losses in the cell. Thus the simultaneous goals of improving power density while lowering the operating temperature are at odds with each other. Therefore, the focus of recent research is aimed at development of more active electrodes and more conductive electrolyte materials that can efficiently operate at lower temperatures (600–800°C).

A very large fraction of the total polarization losses is known to occur at the electrode-electrolyte interfaces manifesting itself as the kinetic barrier to redox reactions. Great advances have been made in reducing this polarization loss at the electrodes through the use of two-phase porous composite electrodes [1–4] and mixed conducting electrodes [5]. Much of this work has been aimed at developing electrodes for SOFCs based on the conventional yttria stabilized zirconia (YSZ) electrolyte. The focus of this paper is an investigation of cathode materials for SOFCs based on the perovskite

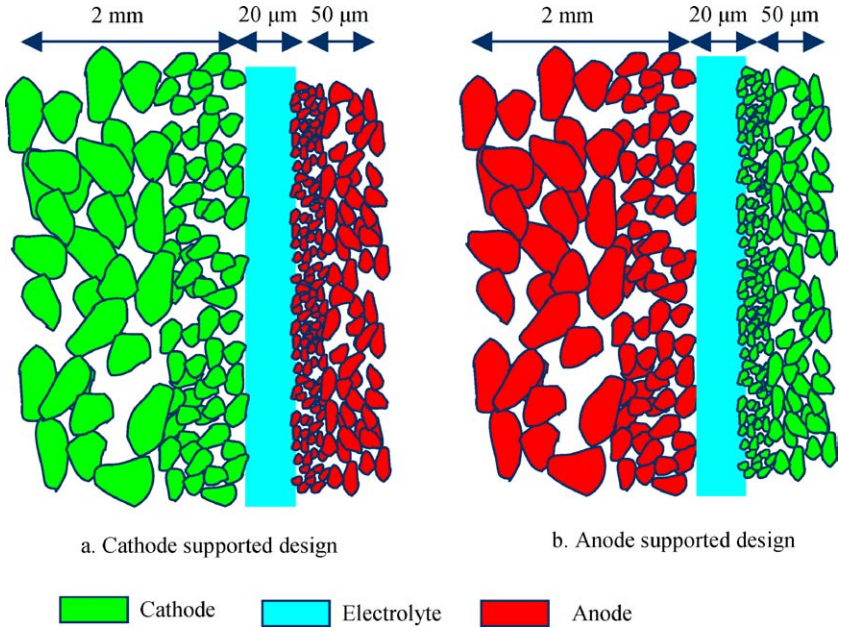

Fig. 1. Schematics of electrode-supported SOFCs.

electrolyte LSGM. LSGM has received a lot of interest in recent years after it was first reported by Goodenough et al. [6] to have significantly higher oxygen-ion conductivity than conventional YSZ.

It is generally accepted that high power densities in SOFCs can be achieved only through employment of electrode-supported cells rather than electrolyte-supported cells. There are essentially two options in the design of electrode-supported cells, namely, cathode- and anode-supported SOFCs. Schematics of the two designs are shown in Fig. 1. In both designs, it is suggested that coarser-grained electrodes with coarser connected porosity be employed away from the electrolyte-electrode interfaces while finer-grained electrodes with finer connected porosity used closer to the electrolyte-electrode interfaces. The coarser porosity away from the electrolyte-electrode interface facilitates gas transport and the finer porosity closer to the interfaces aids in the redox reactions. Henceforth we will use the term interfacial polarization to refer to the redox polarization loss. This paper reports measurements of interfacial polarization resistances for various materials for potential application as the finer microstructured layer near the electrolyte-cathode interface as shown in Fig. 1.

Experimental

The list of electrode materials investigated in this study is given in Table 1.

Powder Synthesis

Electrolyte powders of the composition $La_{0.9}Sr_{0.1}Ga_{0.8}Mg_{0.2}O_3$ (LSGM) were synthesized by mixing and ball-milling high purity precursors of lanthanum carbonate, strontium carbonate, gallium oxide and magnesium oxide in appropriate stoichiometric ratios and calcining at a temperature of 1200°C for 4 hours in air. Electrode

Table 1. The list of electrode materials investigated and the respective thickness.

Electrode materials	Pt	LSM	LSM-LSGM	LSCF
Composition	Pure Platinum	Pure $La_{0.9}Sr_{0.1}MnO_3$	$La_{0.9}Sr_{0.1}MnO_3$ $+La_{0.9}Sr_{0.1}Ga_{0.8}Mg_{0.2}O_3$	Pure $La_{0.6}Sr_{0.4}Co_{0.8}Fe_{0.2}O_3$
Thickness (μm)	5	30	30	4.5 to 150

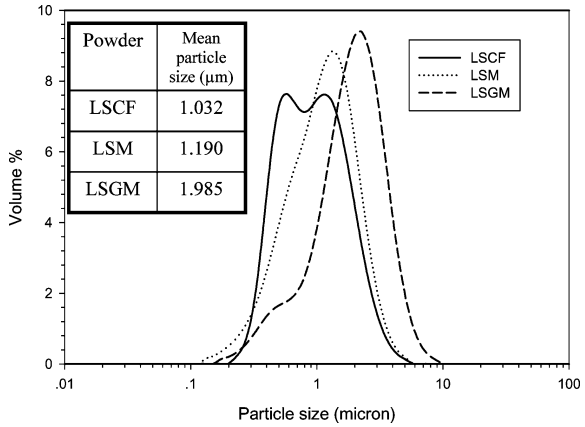

Fig. 2. Final particle size distribution of the synthesized powders.

materials such as $La_{0.9}Sr_{0.1}MnO_3$ (LSM) and $La_{0.6}Sr_{0.4}Co_{0.8}Fe_{0.2}O_3$(LSCF) were also made using the same mixing and calcination techniques. The calcined powders were lightly crushed using alumina mortar and pestle and the calcination step was repeated for completing the solid-state reaction. X-ray powder diffraction analysis confirmed the composition, phase and purity of the material. All the synthesized powders (LSGM, LSM, LSCF) were then separately ball-milled for 24 hours in methanol. Laser Scattering Particle Size Distribution Analyzer (Horiba LA-910) was periodically used at different intervals of the ball milling process to determine the particle size and distribution. The ball milling process was stopped when the desired particle size and distribution were obtained. The final particle size and distribution of all the powders are shown in Fig. 2.

Symmetrical Cell Fabrication

Calcined and milled LSGM powders at room temperature were die-pressed with 10000 psi pressure into pellets and sintered in air at 1450°C for 4 hours. The sintered LSGM pellets were 1.4 mm thick and 2 cm in diameter. The LSGM pellets were then all finely ground to a uniform 1 mm thickness using diamond grinding discs. LSM-LSGM composite electrodes were prepared by thoroughly mixing controlled amounts of LSM and LSGM powders. The electrode powders (LSM, LSM-LSGM, LSCF) were each dispersed in α-terpeniol solvent to form a paste. The ground LSGM electrolyte pellets were masked with Scotch^{TM} tape to form an outer ring on both sides and the electrode pastes were painted smoothly on the open circular surfaces. The painted electrolyte pellets were air dried, masks removed and fired in air at 1100°C for 2 hrs. To obtain different electrode thicknesses, the electrodes were painted multiple times followed by a final firing step. When platinum electrodes were used, commercial platinum paste (6926 Engelhard) was painted over a similarly masked LSGM electrolyte pellet, air dried, masks removed and fired at 950°C for 2 hrs. All electrodes had the same effective area of around 1.33 cm^2. Two pieces of platinum mesh were co-sintered on both electrode surfaces at the same time to act as current collectors. Pt lead wires were used to connect the platinum mesh current collectors to the measuring instrument.

AC Impedance Characterization

AC complex impedance spectroscopy has been used to measure the effective interfacial polarization at the cathode-electrolyte interfaces using symmetrical cell arrangements.

The experimental setup that was used is shown in Fig. 3. In this setup the symmetrical cell is exposed to air on both sides and a two-probe configuration was used to measure the impedance spectra. During the measurements a constant flow of 200 cc/min air was maintained over the electrodes. The measurements were made by applying a small-amplitude AC voltage (10 mV) to the cell and monitoring the response current as a function of the AC frequency (from 1 mHz to 65 KHz). Impedance measurements were made in the temperature range of 600 to 800°C in 50°C increments for all the samples using a Perkin-Elmer potentiostat/galvanostat (263A) and solartron analytical frequency response analyzer (model 1250).

These impedance measurements were performed both as a function of composition for LSM-LSGM electrodes and as a function of electrode thickness for the LSCF electrodes. After electrochemical testing, SEM pictures of the samples were taken for microstructural investigation. Both SEM and optical microscopy were used to measure the thickness of the electrodes and confirm the consistency of the structure in terms of grain size and porosity.

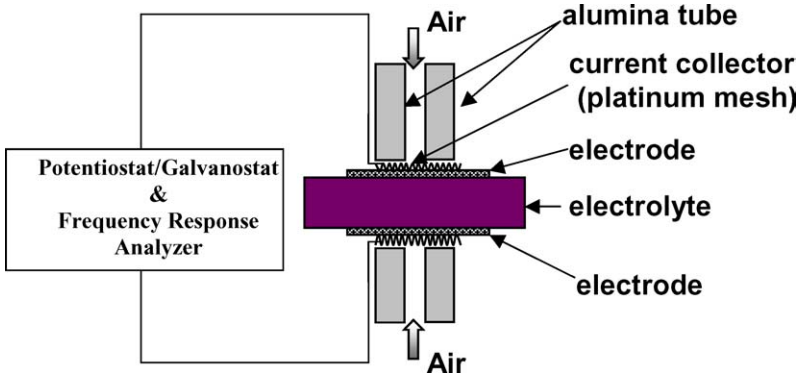

Fig. 3. A schematic diagram showing the experimental setup of symmetrical cells for impedance measurements.

Results and Discussion

Microstructure

Typical SEM micrographs of the fracture surfaces of the electrodes LSM, LSM-LSGM, LSCF and their interfaces with the electrolyte are shown in Fig. 4. The cross sections in Fig. 4 show that these electrodes have similar microstructures in terms of their interfacial adherence with the LSGM electrolyte, porosity and grain size. The grain size is on the order of 1–2 μm and based on the porosity gas diffusion is not expected to control the polarization process particularly for small applied potentials that were used for the AC impedance measurements.

Impedance Spectroscopy

A typical impedance plot measured using the symmetrical cell arrangement with LSCF electrodes is shown in Fig. 5. As discussed elsewhere by previous workers [7–13], the high-frequency intercept of the impedance spectrum gives the ohmic resistance of the cell (R_s), which includes the resistive contributions of the electrolyte, the two electrodes, the current collectors and the lead wires. The low-frequency intercept gives the total resistance ($R_s + R_p$), which includes the ohmic resistance of the cell, concentration polarization (or mass transfer polarization) resistance and the effective interfacial polarization resistance ($R^{\text{eff}}_{\text{redox}}$). The total polarization resistance of the electrode (R_p) is then extracted from the impedance plot. For all samples measured in this investigation, a single depressed arc was observed. Given that the electrodes are thin, the amplitude of the applied AC voltage is small (10 mV), and the air flow over the electrode was continuous, it is most likely that the effective interfacial polarization resistance, $R^{\text{eff}}_{\text{redox}}$, dominates the polarization resistance for the electrodes, i.e. the concentration polarization is negligibly small and R_p is essentially equal to $R^{\text{eff}}_{\text{redox}}$.

Effect of LSM-LSGM Electrode Composition on Polarization Resistance

The typical AC impedance spectra of LSM-LSGM/LSGM/LSM-LSGM symmetrical cells (with about 30 μm thick electrodes) tested at 800°C in air are shown in Fig. 6. It is evident from this figure that when the LSGM content in the electrode is below 70 w%, the high frequency intercepts remained the same, indicating that the ohmic resistance of the cell was dominated by the electrolyte contribution. However, within this limit an increase in the LSGM content resulted in a decrease of the polarization resistance, which was due to the increased mixed conducting TPB area within the electrode. When the LSGM content was more than 70 w%, the ohmic resistances of the electrodes were no longer negligible indicating that the electronic conducting paths were no longer percolating. This is evident from the much larger high-frequency intercept of the impedance spectra for these cells (Fig. 6). The temperature dependence of the polarization resistance for different LSM-LSGM compositions is shown in Fig. 7. The activation energies as a function of LSM-LSGM composition obtained from Fig. 7 are shown in Table 2. The activation energies increased with the LSGM content, from 126 KJ/mol for pure LSM to 182 KJ/mol for the 40/60 LSM-LSGM electrode. The exact reasons for this are not clear at the present time.

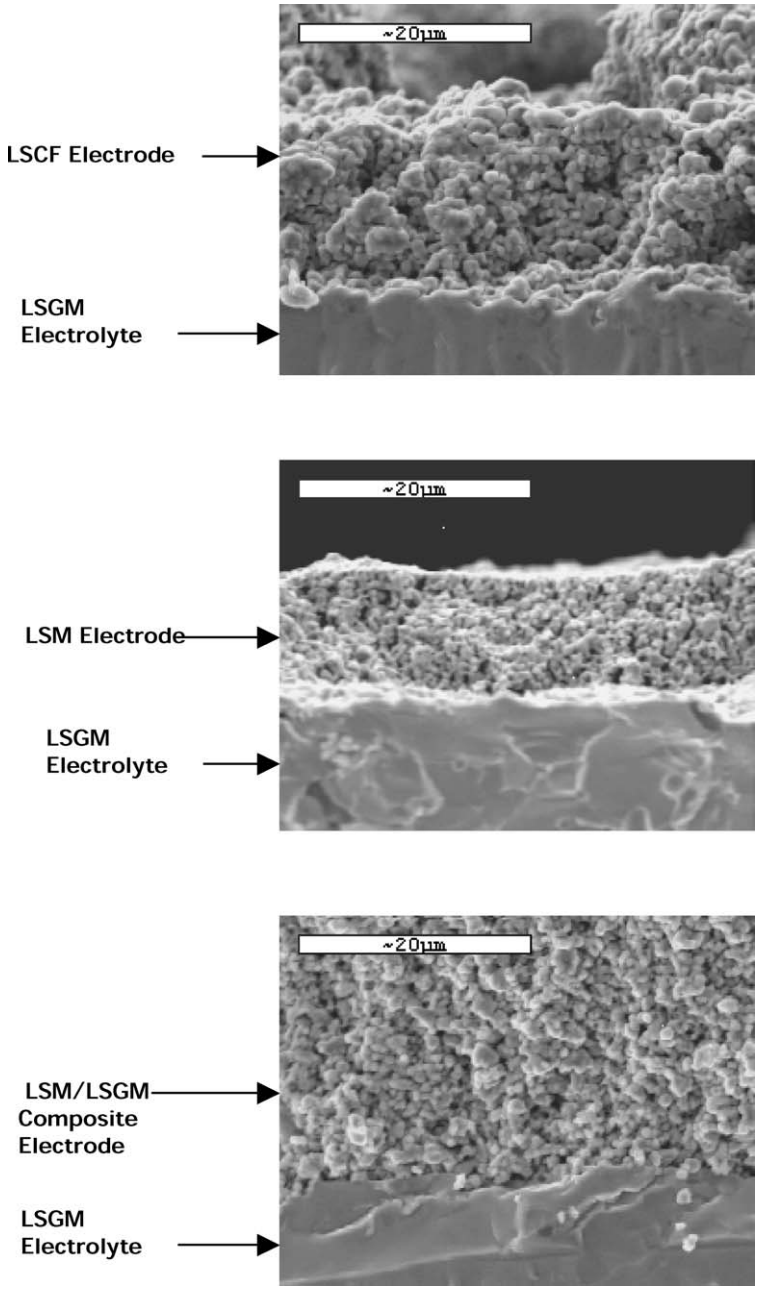

Fig. 4. SEM micrographs of fracture surfaces of (a, top) LSCF/LSGM interface, (b, middle) LSM/LSGM interface, (c, bottom) LSM-LSGM/LSGM interface.

Effect of Electrode on Polarization Resistance

The Arrhenius plot of the measured polarization resistances for the various cathode materials, listed in Table 1, are shown in Fig. 8. It is to be noted that the ohmic resistances, R_s, obtained from the high-frequency intercepts of the impedance spectra, were approximately the same for all these electrodes indicating that the effective electrode/electrolyte interfacial contact areas for these electrodes were similar. As can be seen in Fig. 8, the standard 30 μm thick LSM cathode has a polarization resistance which is

Table 2. Activation energies of LSM-LSGM composite electrodes on LSGM electrolyte.

	Pure LSM	LSM-LSGM 90:10	LSM-LSGM 80:20	LSM-LSGM 70:30	LSM-LSGM 60:40	LSM-LSGM 50:50	LSM-LSGM 40:60
Ea (KJ/mol)	126	156	155	165	168	167	182

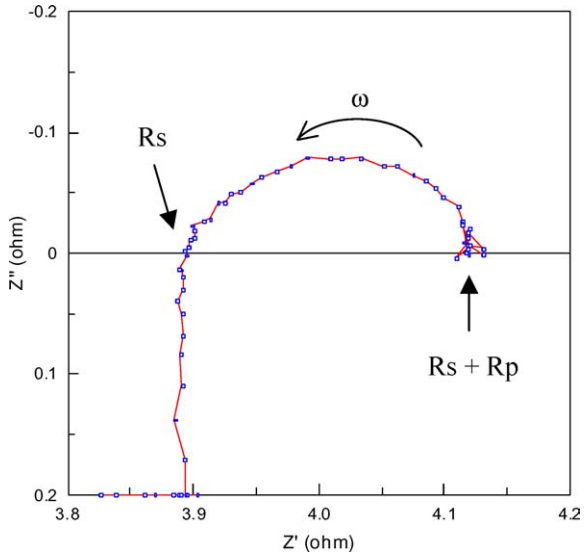

Fig. 5. A typical impedance of symmetrical LSCF/LSGM/LSCF cell in air at 800°C.

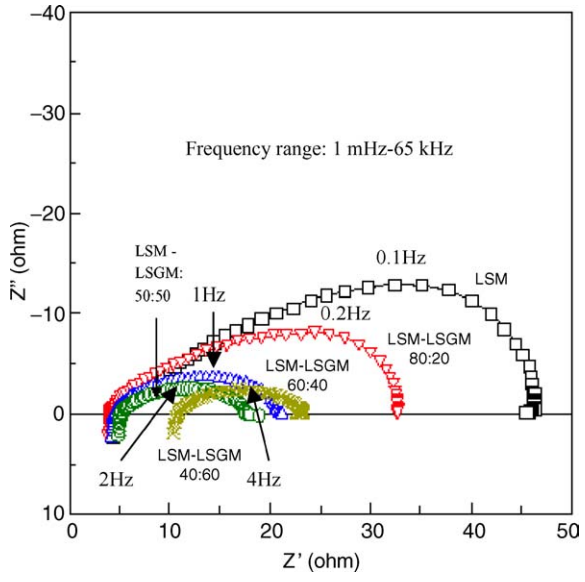

Fig. 6. Typical impedance spectra of symmetrical LSM-LSGM/LSGM'LSM-LSGM cells with different LSM-LSGM compositions measured in air at 800°C.

Table 3. Activation energies of investigated electrodes on LSGM electrolyte.

	Pure LSM	LSM-LSGM 40:60	Platinum	LSCF
Ea (KJ/mol)	126	182	163	165

worse than the 5 μm thick Pt electrode. The 30 μm LSM-LSGM (40:60) composite electrode has a polarization resistance that is very similar to the Pt electrode. In contrast the 30 μm thick LSCF electrode has a polarization resistance which is six orders of magnitude lower than the Pt, LSM and LSM-LSGM electrodes. The activation energies of these electrodes are listed in Table 3. These values do suggest that both the catalytic behavior and the ionic conduction constituent of the electrodes influence the activation energies.

Effect of LSCF Electrode Thickness on Effective Interfacial Polarization Resistance

AC impedance spectra of LSCF/LSGM/LSCF symmetrical cells at 600°C as a function of electrode thickness are shown in Fig. 9. All the impedance arcs as stated earlier appeared to be nearly semicircle in shape, and the polarization resistance changed with the thickness of the electrodes. It is evident from Figs. 9 and 10 that increasing the electrode thickness has the effect of decreasing the effective interfacial polarization resistance. A similar thickness effect has been observed previously by Kenjo et al. [2, 14] and Tanner et al. [15, 16]. Tanner et al. [15] developed a comprehensive model to explain the thickness effect of the effective interfacial polarization resistance of LSM-YSZ composite electrodes on YSZ electrolytes. When the electrocatalyst cathode is a pure electronic conductor like LSM, the sites for redox reactions have been conclusively shown by Horita et al. [17] using oxygen-18 isotope and secondary ion mass spectrometry (SIMS) to be the three-phase boundaries (TPBs) formed between the electrode (LSM), electrolyte (YSZ) and the

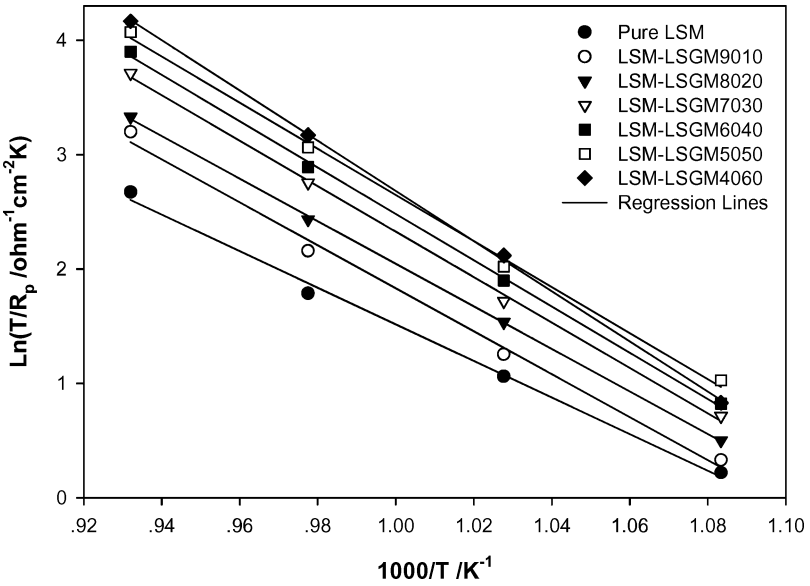

Fig. 7. Temperature dependence of the polarization resistance for different LSM-LSGM compositions measured in air.

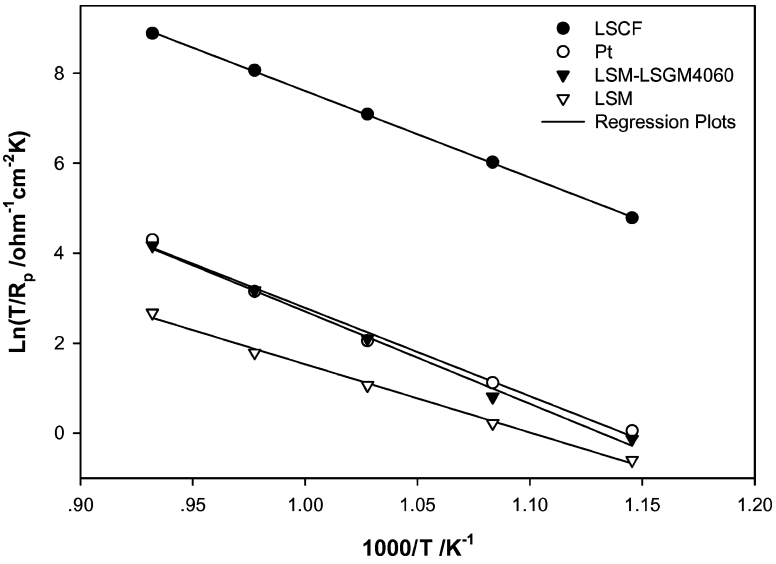

Fig. 8. Temperature dependence of the polarization resistance for various cathode materials measured in air.

gas-phase. Thus, in the case of a porous composite electrode comprising an electrocatalyst phase (LSM), and an ionic conducting phase (YSZ) it is reasonable to expect that increasing the electrode thickness should lead to an increase in the TPB line length and therefore a decrease in effective interfacial polarization resistance eventually approaching an asymptotic minimum. Indeed the experimental and theoretical work of Tanner et al. [15, 16] showed just such a thickness effect.

In the case of a single-phase mixed ionic and electronic conducting (MIEC) electrode, in addition to the TPBs at the electrode-electrolyte interface, oxygen exchange can occur over the entire pore surface area of the electrode. The nature of this oxygen exchange, i.e., whether it is electrochemical or simply a chemical

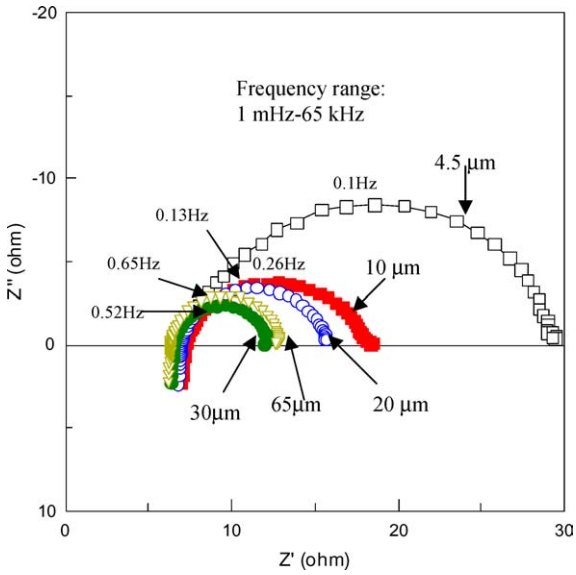

Fig. 9. Impedance spectra of symmetrical LSCF/LSGM/LSCF cells with various electrode thickness measured in air at 600°C.

exchange process is the subject of much recent debate [18, 19]. The results presented here do not throw light on this debate. However, regardless of the nature of the oxygen exchange process, an increase in MIEC electrode thickness should reduce the total polarization resistance by increasing the number of sites available for exchange between the gas phase and the electrode-electrolyte system just as in the case of porous composite electrodes [15]. As can be seen from Fig. 10, this is indeed the case observed in this study involving the LSCF/LSGM/LSCF symmetrical cells. Figure 10 also shows a fit to our data employing the model developed by Tanner et al. [15] using assumed values of porosity (30%), intrinsic polarization resistance for the oxygen redox resistance R_{redox} ($1.2\ \Omega \cdot \text{cm}^2$) and grain size ($1\ \mu$m). This also confirms our initial hypothesis that concentration polarization is a minor contributor to the total polarization resistance in our experiments. Upon further increasing the electrode thickness, pore diffusion of molecular oxygen through the MIEC electrode phase may become rate controlling and therefore increase the total electrode polarization resistance. Indeed, this effect has been predicted by Tanner et al. [15]. However, such an increase was not observed in the electrode thickness range investigated in this study (4.5 to 150 μm). This once again confirms our hypothesis that the electrodes investigated in this study were not rate-controlled by gas-phase pore diffusion.

The effect of microstructure changes on effective interfacial polarization resistance has not been investigated in this study. But, it can be expected that a finer micro-structured electrode is expected to lead to a lower

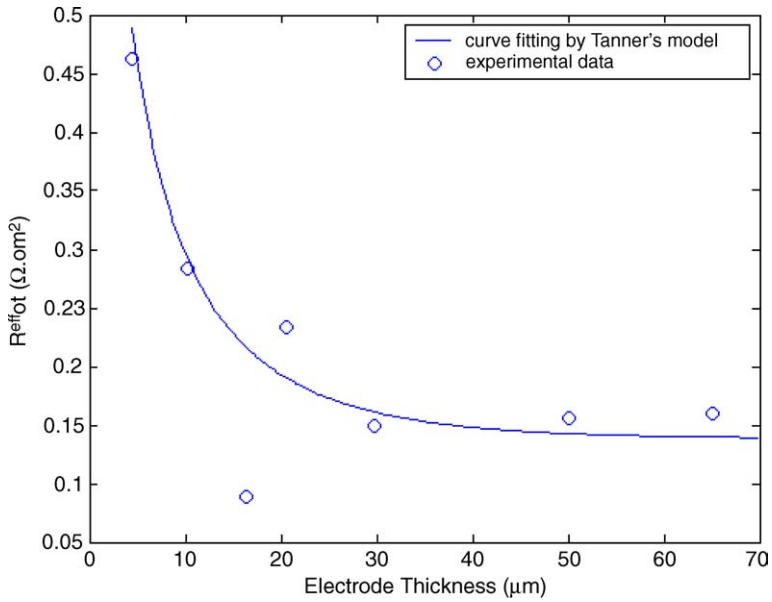

Fig. 10. A plot of interfacial polarization resistance as a function of electrode thickness for symmetrical LSCF/LSGM/LSCF cells measured in air at 800°C.

effective interfacial polarization resistance due to the availability of greater number of sites for redox reactions. As shown theoretically by Tanner et al. [15], the thickness at which the asymptotic minimum in the effective interfacial polarization resistance is attained for a given electrode depends on the microstructure of the electrode; finer the electrode microstructure smaller the electrode thickness at which the asymptotic minimum is attained. This behavior will also be dependent on the mixed conducting characteristics of the electrode. These are some of the other cathodic polarization issues that are being investigated and will be the subject of future publications.

Conclusions

Cathodic-interfacial polarization of several candidate electrodes for LSGM electrolyte has been investigated by impedance spectroscopy technique. Among these electrodes (LSM, LSM-LSGM and LSCF), the pure LSM electrode has the worst polarization performance. The addition of LSGM electrolyte material to the LSM electrode increases the mixed-conducting boundary with the gas phase and lowers the polarization. Although LSM-LSGM composite electrodes are better than just pure LSM, the performance of the best LSM-LSGM (40:60) electrode was similar to that of platinum. Single phase mixed-conducting LSCF electrode has the lowest polarization resistance among the electrodes that were investigated. As expected, the polarization resistance of the LSCF electrode decreased asymptotically as the electrode thickness is increased.

Acknowledgment

This paper was prepared with the support of the US Department of Energy, under Award No. DE-FG26-02NT41539. However, any opinions, findings, conclusion, or recommendations expressed herein are those of the authors and do not necessarily reflect the views of the DOE.

References

1. T. Kawada, N. Sakai, H. Yokokawa, M. Dokiya, M. Mori, and T. Iwata, *J. Electrochem. Soc.,* **137**, 3042 (1990).
2. T. Kenjo and M. Nishiya, *Solid State Ionics,* **57**, 295 (1992).
3. M.J.L. Østergård, C. Clausen, C. Bagger, and M. Mogensen, *Electrochim. Acta* **40**, 1971 (1995).
4. V. Dusastre and J.A. Kilner, *Solid State Ionics*, **126**, 163 (1999).
5. M.T. Colomer, B.C.H. Steele, and J.A. Kilner, *Solid State Ionics*, **147**, 41 (2002).
6. M. Feng and J.B. Goodenough, *Eur. J. Solid State Inorg. Chem*., **31**, 663 (1994).
7. H. Hu and M. Liu, *Solid State Ionics*, **109**, 259 (1998).
8. S. Wang, X. Lu, and M. Liu, *J. of Solid State Electrochemistry*, **6**, 384 (2002).
9. S.B. Adler, *Solid State Ionics*, **111**, 125 (1998).
10. Paola Costamagna, Paolo Costa, and Vincenzo Antonucci, *Electrochimica Acta*, **43**, 375 (1998).
11. A. Barbucci, R. Bozzo, G. Cerisola, and P. Costamagna, *Electrochimica Acta,* **47**,2183 (2002).
12. J.E. Bauerle, *J. Phys. Chem. Solids*, **30**, 2657 (1969).
13. J.R. Macdonald, *Impedance Spectroscopy: Emphasizing Solid Materials and Systems* (Wiley, New York, 1987).
14. T. Kenjo, S. Osawa, and K. Fujikawa, *J.Electrochem. Soc.*, **138**, 349 (1991).
15. C.W. Tanner, K.Z. Fung, and A.V. Virkar, *J. Electrochem. Soc.*, **144**, 21 (1997).
16. A.V. Virkar, J.Chen, C.W. Tanner, and J.W. Kim, *Solid State Ionics*, **131** 189 (2000).
17. Teruhisa Horita, Katsuhiko Yamaji, Natsuko Sakai, Yueping Xiong, Tohru Kato, Harumi Yokokawa, and Tatsuya Kawada, *Applied Surface Science,* **203–204**, 634 (2003).
18. Meilin Liu and Zhonglin Wu, *Solid State Ionics*, **107**, 105 (1998).
19. S.B. Adler, J.A. Lane, and B.C.H. Steele, *J. Electrochem. Soc.*, **143**, 3554 (1996).